Morphology and Distribution Structure Characterization of Methane Hydrate Formed in the Presence of Amphiphilic Antiagglomerant Additive

Mohamad Abdallah, Thibaud Chevalier, Maxime Pelerin, Anne Sinquin, Annie Fidel-Dufour, Nicolas Lesage, Arnaud Desmedt

Morphology and distribution structure characterization of methane hydrate formed in the presence of amphiphilic anti-agglomerant additive.

Mohamad Abdallah[a,b,c], Thibaud Chevalier[a,*], Maxime Pelerin[a], Anne Sinquin[a], Annie Fidel-Dufour[c], Nicolas Lesage[c] and Arnaud Desmedt[b,d]

[a] IFP Energies nouvelles, 1-4 Avenue de Bois-Préau, 92852 Rueil-Malmaison, France
[b] Groupe Spectroscopie Moléculaire, ISM, UMR 5255 CNRS, Univ. de Bordeaux, Talence, FR.
[c] TotalEnergies OneTec, CSTJF, Avenue Larribau, 64018 Pau, France
[d] Laboratoire Léon Brillouin, UMR12 CNRS, CEA Saclay, Gif sur Yvette, France

Corresponding author(s): thibaud.chevalier@ifpen.fr

ABSTRACT

We investigate the impact of commercial amphiphilic anti-agglomerant additive (AA) on hydrate crystals morphology, size and dispersion in organic phases, by using optical imaging and Raman spectroscopy. To better reproduce the conditions during oil and gas offshore production, methane hydrates were formed from saline water (5 g/L NaCl) in the presence of AA additive at various concentrations (aqueous solutions of 5 and 7 % wt), by using Ketrul211® condensate phase (corresponding to a petroleum cut of C_{12}-C_{14} carbon distribution), under a constant subcooling of 8.5 ± 0.5 K and 70 bar. Two systems have been studied: water-AA/methane and water-AA/ketrul211®/methane. By optical imaging observation, the presence of AA additives leads to polygonal periodic crystals (with size ranging from *ca*. 1 to 10 µm) for the water-AA/methane system, and perpendicular needle crystals (with size close to 10 µm) for the water-AA/ketrul211®/methane system. In the absence of AA additive, no polygonal or needle crystals morphology has been observed. With the help of Raman imaging, the methane hydrate distribution has been investigated at a micrometer scale: the formation of methane hydrates aggregates is revealed inside the ketrul211® bulk phase matrix.

I- Introduction

Gas hydrates are non-stoichiometric crystalline solids formed from liquid water and low molecular weight gases at high pressures and low temperatures. There are 3 types of gas hydrates unit structures, where hydrates structure SI encapsulates the smallest gas species (such as methane, ethane or carbon dioxide …), hydrates structure SII encapsulates gas molecules up to the size of propane and iso-butane, and hydrate structure SH encapsulates larger hydrocarbon molecules such as iso-pentane and n-hexane[1].

Gas hydrates constitute major challenge for offshore oil and gas operation fields, where hydrates deposits can block flow lines and cause production shut down. Many different strategies have been developed for hydrate management, such as production outside gas hydrate stability zone, pipeline electrical heating, line insulation, gas dehydration and thermodynamic hydrate inhibitors (THIs)[2]. These last decades, alternative chemical injection strategies have been developed, such as low dosage hydrate inhibitors (LDHIs). They are divided in two categories: kinetic hydrate inhibitors (KHIs) and anti-agglomerant additives (AAs). KHIs mechanisms consist in delaying gas hydrates nucleation and slowing down the growth of hydrate crystals. AAs mechanisms consist in preventing hydrates agglomeration and allowing hydrate particles to be dispersed in the hydrocarbon phase and/or water phase[3-6]. In the literature, KHIs mechanisms have been largely studied[7], but, even if some AAs were tested or deployed on fields[8,9], research is still required to investigate AAs[10-11] dosage, mechanisms and performances as a new technical solution for hydrate anti-agglomeration strategy and fields' lifetime extension.

Raman spectroscopy is an experimental approach, particularly appropriated for investigating gas hydrate formation[1,2]. In the case of studies performed on methane hydrate formed without organic phase, without additives and without agitation, it has been shown that gas hydrate grows at the water/gas interface, leading to an impermeable and non-porous crust film[12-14]. Regarding the formation with additives, several studies have focused on water/methane system with sodium dodecyl sulfate (SDS®) surfactant – at concentrations as low as 500 ppm. With the SDS additive, the water/methane mass transfer can be maintained at the interface between water and gas phases[15-19] leading to the formation of a compact hydrate crystal with 60 - 80 % porosity and 20-30 µm pores size. The SDS® surfactant - considered as a hydrate promoter -impact the hydrate formation and its porosity[20]. Raman spectroscopy is an experimental approach, particularly appropriated for investigating gas hydrate formation. In the present study, the impact of commercial AAs additives on hydrate crystals morphology and aggregate size have been investigated by using Raman spectroscopy and optical imaging.

Complementary measurements (Differential Scanning Calorimetry, Tensiometry and Thermodynamics calculations) have been carried out for complementing the in-depth understanding of the impact of AAs on hydrate crystal size and dispersion in ketrul211® phase. To better reproduce the conditions during a natural gas production, methane hydrates were formed from saline water (5 g/L NaCl) in the presence of operational anti-agglomerant additive at various concentrations (aqueous solutions of 5 and 7 % wt). Hydrate formation has been performed inside thin capillary (200µm diameter) and Raman micro-spectroscopy has been carried out to *in-situ* image the hydrate formation at 70 bar and at 274.15 K at a micrometer scale. The natural gas hydrates have also been formed in the presence of AAs additives inside macroscopical reactors and camera-analyzed to check that the characteristic hydrates morphology was similar in a macroscopic reactor and in a micrometric capillary. Finally, in order to better mimic the chemical composition met in multiphase flow loop[21-22], methane hydrates accumulation and morphology were studied not only in two phase's system (water/methane) but also in triphasic system (water/ketrul211®/methane).

II- Experimental details

Ultra-pure Milli-Q water has been used to prepare the aqueous solution with 5 g/L sodium chloride and 5 or 7 % weight concentration of amphiphilic anti-agglomerant additive (AA), supplied by TotalEnergies (commercial formulation containing quaternary ammonium – information from Safety

Data Sheet).The condensate phase used is the solvent Ketrul211® provided by TotalEnergies. It is an iso-paraffinic petroleum cut, its distillation's temperature's range between 485 and 516 K corresponding to C_{12}-C_{14} carbon distribution. This solvent has a density of 814 kg/m^3.

Superficial and interfacial tensions were measured on the systems using K100 tensiometer from Krüss and spinning drop tensiometer (SVT 20N, Dataphysics). The AA additive significantly lowers the aqueous solution/ketrul211® interfacial tension from 42.00 to 0.81 mN/m, and the aqueous solution/air superficial tension from 65.79 to 29.20 mN/m (Table 1). These results indicate the presence of AA molecules at the interfaces between aqueous solution and ketrul211® as well as between aqueous solution and air.

Table 1 : Surface tension and interfacial tension measurements.

Aqueous phase (5g/L NaCl)	Superficial tension aqueous phase/air (mN/m)	Interfacial tension aqueous phase/ketrul211® (mN/m)
without additive	65.79	42.00
1 % wt. AA additive	29.20	0.81

The AA additive critical micellar concentration (CMC) was also determined using K100 tensiometer from Krüss, and the value obtained is 0.004 % wt. From this result, it can be concluded that for a concentration of 1, 5 or 7% wt. of AA additive, the water/methane and water/ketrul211® interfaces are saturated by AA molecules, and the water phase contains micelles of AA additive.

The impact of the AA additive on a natural gas hydrate equilibrium condition has been explored using µDSC VII® (differential scanning calorimeter from Kep Technologies). For water/natural gas system, the presence of 1 % wt. AA additive leads to gas hydrate structure SII dissociation temperature at 288.15 ± 0.5 K. In the absence of AA additive, the natural gas hydrate dissociation temperatures have been measured at 281 and 288 ± 0.5 K for gas hydrate structures SI and SII respectively. By these results, only gas hydrate structure SII has been formed in the presence of AA additive. It can be considered that the AA additive, has no thermodynamic impact on the natural gas hydrate structure SII dissociation. In complementary, the Multiflash®6.1 has been used and the natural gas hydrate dissociation temperatures has been calculated at 281.15 and 288.25 ± 0.5 K for structures SI and SII respectively. These simulated values can be considered close to measured dissociation temperatures values obtained by µDSC VII®.

As shown in Figure 1, *in-situ* experiments have been performed using the Xplora confocal microspectrometer (Horiba Jobin Yvon) at 532 nm incident wavelength with a grating of 600 lines/mm (leading to a spectral resolution of *ca*. 3 cm^{-1}). A 50x objective has been used for acquisitions, allowing to reach micrometer spatial resolution in Raman imaging. The Raman images have been recorded in a 40 x 30 µm^2 area with a 1 µm step, corresponding to the acquisition of 1200 Raman spectra in the probed area. The acquisition time per spectrum was 20 *sec*, leading to acquisition time of *ca*. 7 hours for a full Raman image.

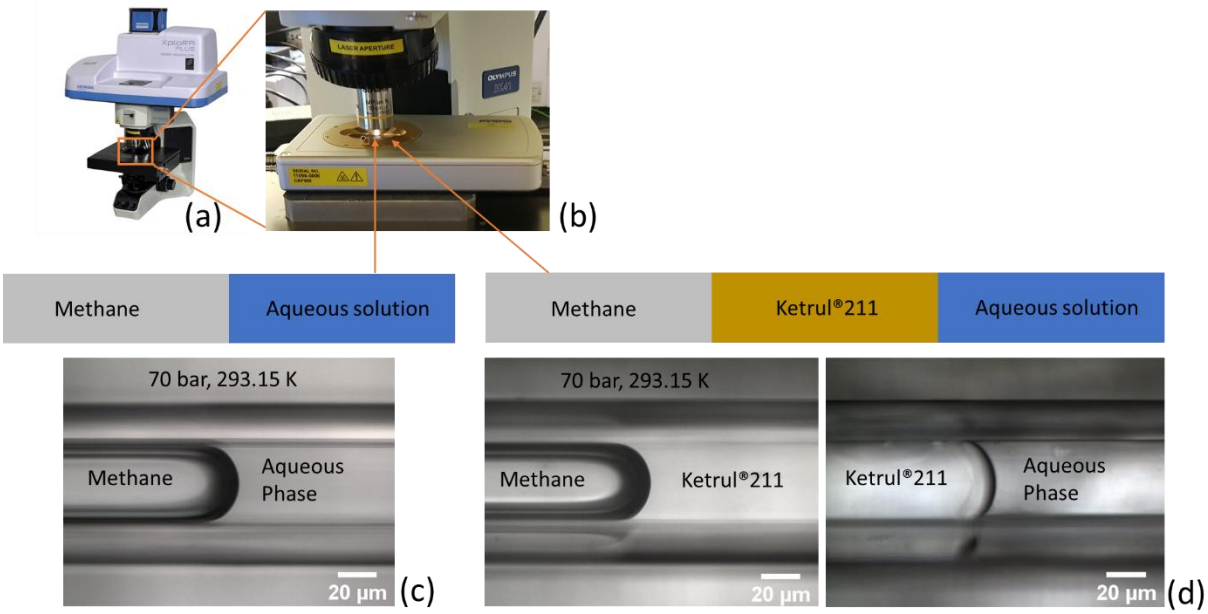

Figure 1 : (a) Xplora microspectrometer (Horiba Jobin Yvon). (b) CAP500 Linkam stage within which capillaries were inserted. Optical images of the water/methane system (c) and of the water/ketrul211®/methane system (d).

Square quartz capillary, supplied from CM scientists (200 µm inner diameter, 400 µm outer diameter, 100 mm length) was used to form the methane hydrates. The capillary was connected to a high-pressure syringe pump allowing to work at constant pressure and the temperature was controlled thanks to a Linkam CAP500 liquid nitrogen stage, within which the capillary was inserted. All the samples have been loaded in the capillary at atmospheric pressure and ambient temperature. For all systems presented in the next section, we acquired optical images before and after hydrate formation along the capillary, with a focus on the different interfaces/phases: as illustrated on Fig. 1 (c) and (d) the gas is always on the left of the capillary, the aqueous phase on the right and the ketrul211®, if any, in the middle. The images after hydrates formation are taken when no more evolution is detected and the system is stabilized. The methane hydrates have been formed at a constant pressure of 70 bar, by applying a constant cooling rate of 10 K/min from 293 ± 0.1 K to 248 ± 0.1 K, then increasing temperature immediately to 274 ± 0.1 K to melt ice and initiate methane hydrate crystallization under suitable thermodynamic conditions. The dissociation temperature of methane hydrate is 282.5 ± 0.5 K at 70 bar (simulated by Multiflash®6.1). Consequently, the experimental measurements have been conducted at a constant subcooling of 8.5 ± 0.5 K. The subcooling represents the difference between the dissociation temperature and the operational temperature at 70 bar.

All Raman acquisitions have been realized at 274 ± 0.1 K and 70 bar. Two systems have been studied with various additive concentrations (Table 2): methane/water and methane/ketrul211®/water. On each system, two set of measurements have been conducted in the presence of operational amphiphilic anti-agglomerant additive (AA): optical and Raman imaging. In addition to the analysis of the hydrate morphology at a micrometer scale, the hydrates and ketrul211® phases distribution was evaluated and mapped at a micrometer scale.

Table 2 : Chemical composition of the samples probed by optical and Raman techniques. The Methane hydrates to gas and to ketrul211® phases ratio have been estimated from characteristic Raman bands ratio (see text and Supplementary Materials for details).

Samples	AA concentration (% weight)	Methane hydrates to gas phases ratio (%)
methane/water	0	50
methane/water	5	47
methane/water	7	49

Samples	AA concentration (% weight)	Methane hydrates to ketrul211® phases ratio (%)
methane/ketrul211®/water	0	50
methane/ketrul211®/water	7	51

III- Results

Optical imaging: hydrate morphology

For water/methane system without AA additive, the hydrates formation started at the water/methane interface, followed by the formation of a thin hydrate layer at the capillary wall towards the methane phase. Figure 2 (a) shows the initial stage of the system at 70 bar and 293 K. Figure 2 (b) shows the methane hydrate crust separating the aqueous phase and the methane gas phase observed at 70 bar and 274 K.

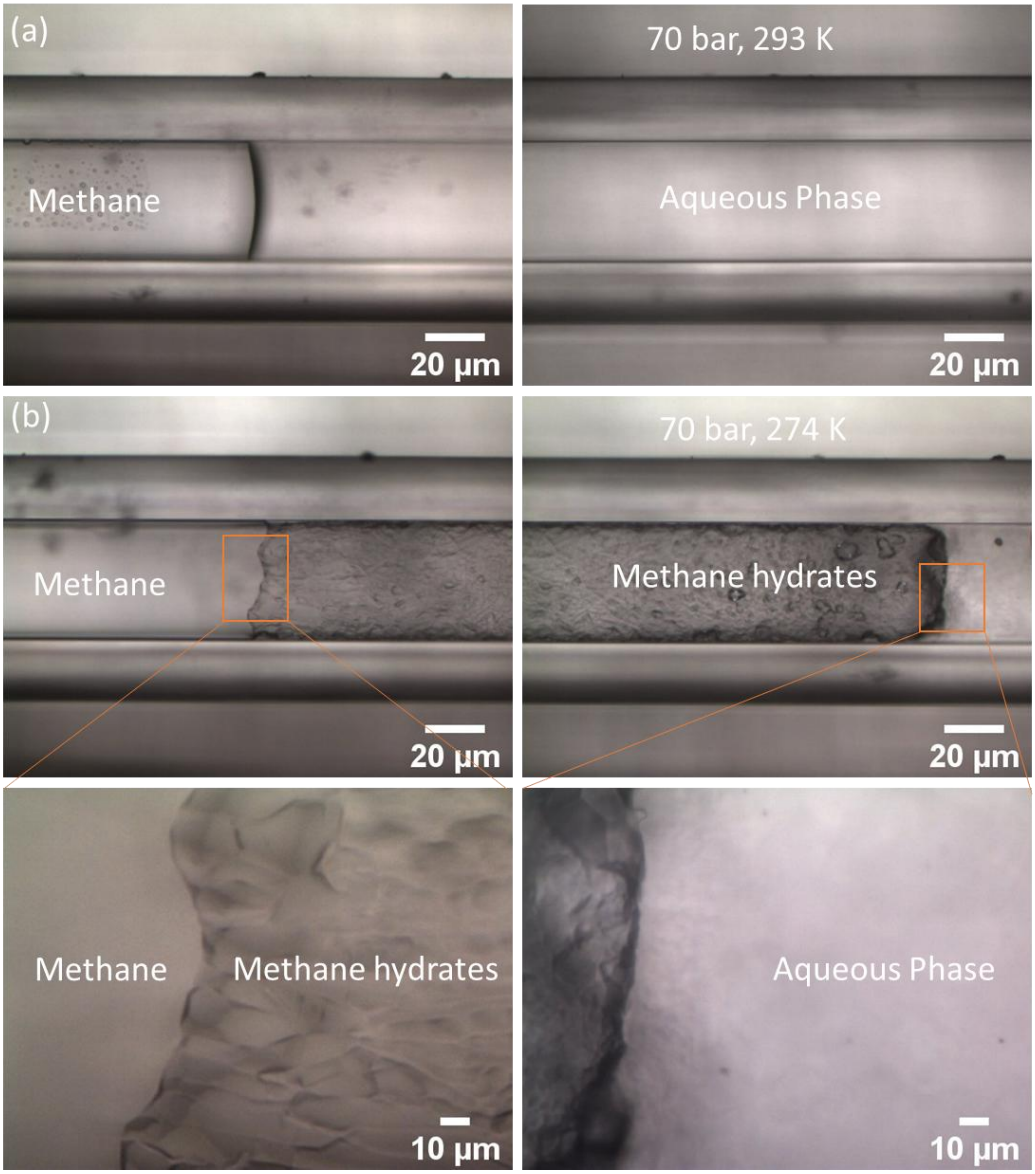

Figure 2 : (a) water/methane liquid interface before the hydrate formation. (b) Methane hydrates formation without AA additive (taken 30 min after the hydrate onset – system stabilized). All temperatures and pressures are indicated on the figure.

For the water/ketrul211®/methane system without AA additive, it has been observed that the methane hydrate developed at the water / ketrul211® interface (Figure 3). A thin hydrate layer has grown from the water/ketrul211® interface toward the ketrul211®/methane interface. This layer covered the entire surface of the quartz capillary in the initial ketrul211® phase (Figure 3). It must be mentioned that this

capillary is hydrophilic. Consequently, the aqueous phase has been drawn up by capillary forces and covered the entire quartz surface at the ketrul211® phase level at atmospheric temperature. Once the pressure and temperature are thermodynamically favorable for hydrate formation and stability, the aqueous layer is converted into methane hydrate layer and after few minutes the crystallization process stopped.

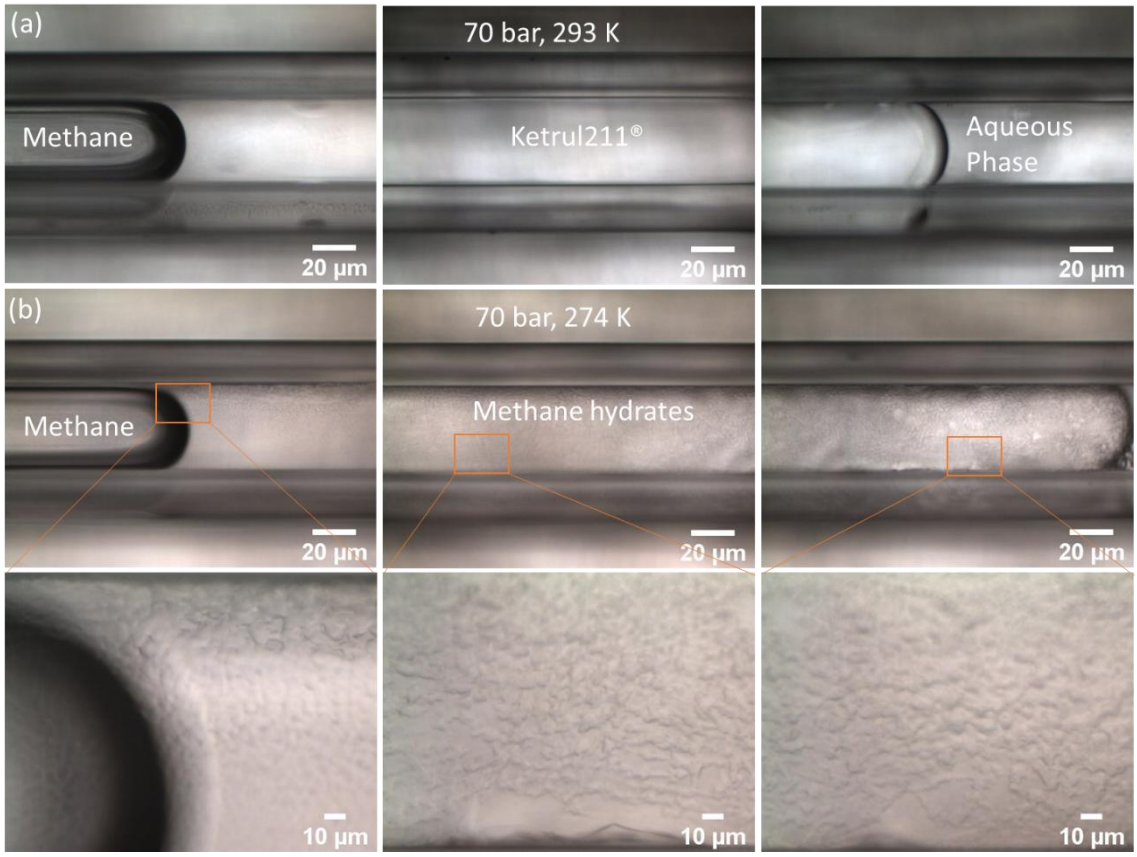

Figure 3 : (a) water/ketrul211®/methane system at 70 bar and 293K. (b) Methane hydrates formation at 70 bar and 274 K in the absence of AA additive (taken 20 min after the hydrate onset – system stabilized).

The impact of AA additive has been investigated for water/methane system. The microscope images (Figure 4) analysis shows the hydrate formation initiation at the methane/water interface. Then, the water phase is drawn up by capillary forces towards the methane hydrate phase and leads to further crystallization as a layer at the capillary wall. The presence of AA additive affords also crystal shape change. Polygonal crystals (with size ranging from *ca*. 1 to 10 µm) are observed in the methane phase (Figure 4). The presence of AA additive leads to 100 % water to hydrate conversion rate. In contrary, the previous system (water/methane without additive) presents unconverted liquid water phase at the end of the capillary: the crystallization has been stopped due to hydrates impermeable layer between water and gas that stops the mass transfer. In comparison, AA additive adsorption mechanism at the water/methane interface leaves fluid mass transfer possible during methane hydrate formation and leads to a complete crystallization. This is consistent with the reduced water/methane surface tension from 65.79 to 29.20 mN/m in the presence of AA additive (Table 1).

For model system, the solute diffusion rate from the bulk to the crystal surface could control the growth rate and shape of the crystalline phase[23]. A slow solute diffusion rate from the bulk water phase to the crystal surface can lead to a slow rate growth, consequently, the crystal tends to develop as a wide surface in multi-direction like polygonal shape[23]. For hydrate system, it has been approved that the low gas diffusion rate led to polygonal crystal morphology[24-25]. However, in this study the polygonal crystals have been developed only in the presence of AA additive (unlike the previous system, water/methane without AA additive). By this, the polygonal morphology is not controlled only by the

methane diffusion rate, but also by the AA additive adsorption mechanism at the water/methane interface.

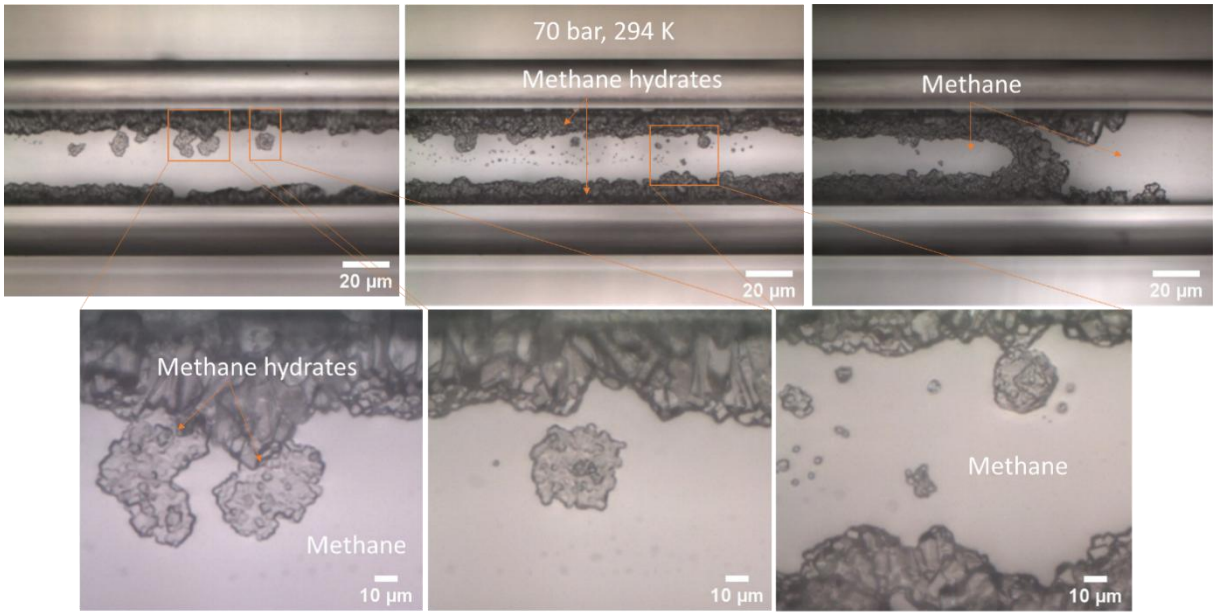

Figure 4 : Methane hydrate morphology in the presence of 7 % wt. AA additive, for water/methane system (taken 2-3 min after the hydrate onset – system stabilized).

The Figure 2 and Figure 4 represent the methane hydrates morphology for water/methane system in the absence and presence of AA additive respectively. The addition of Ketrul211® condensate phase induces totally different methane hydrates crystals shape. For water/ketrul211®/methane system and 7 % wt. AA additive, the methane hydrates formation starts at the water/ketrul211® interface and then, the crystals growth from the interface towards the condensate phase as needles (Figure 5). The process of crystal needles growth is continuous (Figure 6). The presence of AA additive leads for further crystallization (Figure 6), where needles have been developed from water/ketrul211® phase towards ketrul211®/methane phase during about 3 days. It suggests that the AA additive adsorption mechanism keeps methane and water mass transfer through or in the condensate and leads to formation of oil-wet needle crystals.

At the same AA additive concentration (7 % wt.), the crystal morphology changed from polygonal to needle shape by adding the ketrul211® phase. For the water/ketrul211®/methane system, the organic liquid phase was saturated with methane guest molecules. In contrary, for the water/methane system, the methane guest molecules are almost insoluble in the bulk water phase. This different behavior clearly impacts the morphology of the formed crystals. The methane solubility in ketrul211® phase probably increases the methane availability at the hydrate growing surface. The methane solubility and availability in the ketrul211® phase and the AA additive activity at the water/ketrul211® interface keeps the water and methane in contact and leads to needle crystal.

As explained previously, the methane diffusion rate can control the crystal growth rate and morphology[24-25]. The high methane diffusion rate from the bulk liquid phase to the hydrate crystal leads to hydrate growth and thin needle-like crystals. The presence of AA additive tends to develop crystals in a direction perpendicular to the water/ketrul211® interface. As a result, needles are obtained as seen in Figure 5 and Figure 6. Without AA additive, no needle shape is observed. It is obvious that the AA additive (that adsorb on the crystal) has also an impact on the crystal needle shape. The growth mechanism is probably controlled by a competition between the methane diffusion rate and the AA additive adsorption mechanism. The competition between these two phenomena maintains methane and water in contact and lead to crystallization of needle shape crystal.

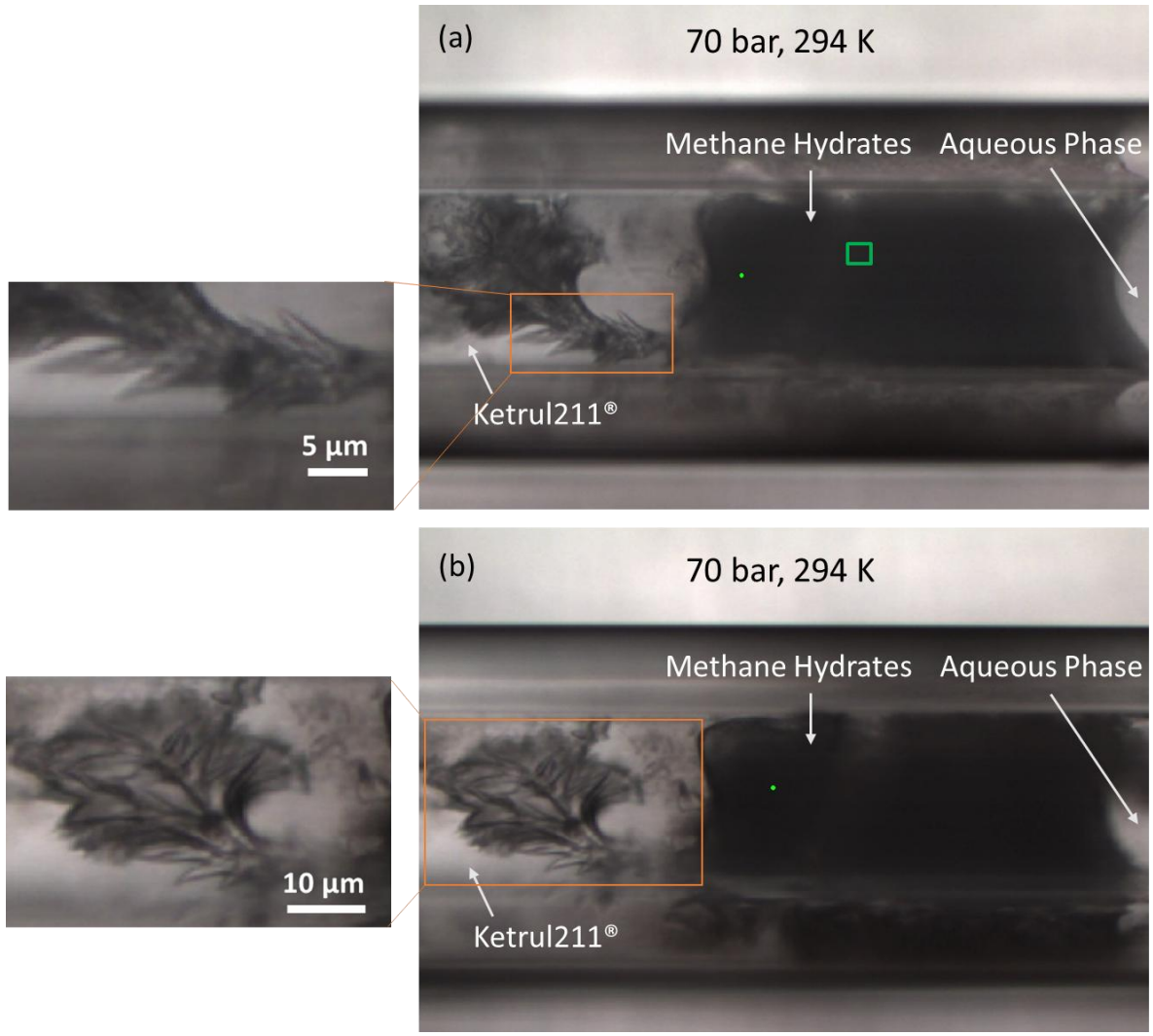

Figure 5 : Methane hydrate morphology in the presence of 7 % wt. AA additive for water/ketrul211®/methane system, at 70 bar and 274 K. For x, y and z axis (a) and (b) refer to the same system, with distinct two positions in the z-axis. (taken 10h after the hydrate onset – system not stabilized).

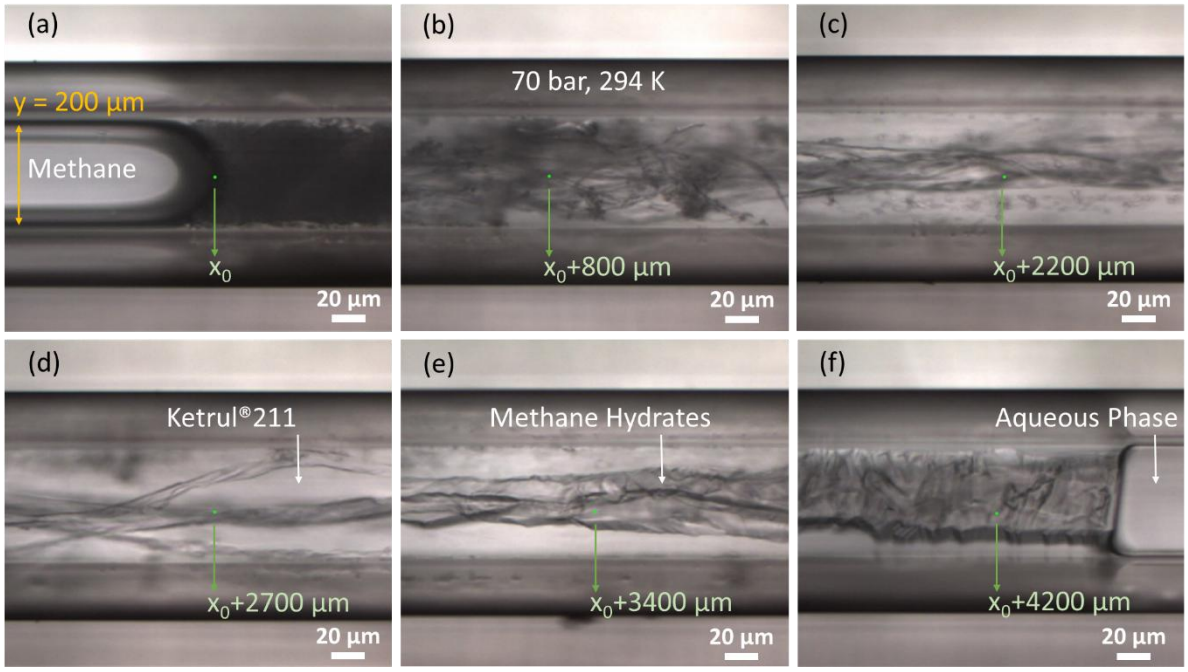

Figure 6 : Needle crystals continuous growth inside capillary in the presence of 7 % wt. AA additive. (a) to (f) refer to the methane/ketrul211®/hydrates/aqueous phases at 70 bar and 294 K with distinct x-axis positions along the capillary (x_0 for the methane/gas hydrate interface position and x_0 + 4200 µm for gas hydrate/aqueous phase interface position. The hydrate growth has been developed over 3 days. The instantaneous evolution could not be detected. Once the system became stable, photos were recorded). (taken 3 days after the hydrate onset – system stabilized).

At macroscopic scale in a high-pressure cell (300 mL), similar needle crystal's morphology has been obtained for a similar crystallization process: the nucleation starts at the water/ketrul211® interface and the needle crystals grow inside the ketrul211® phase (Figure 7). The needle crystal size is in the order of a few millimeters. In conclusion, without stirring, similar needle crystals have been observed at microscopic (with SI pure methane hydrate) and macroscopic scale (with SII natural gas hydrate).

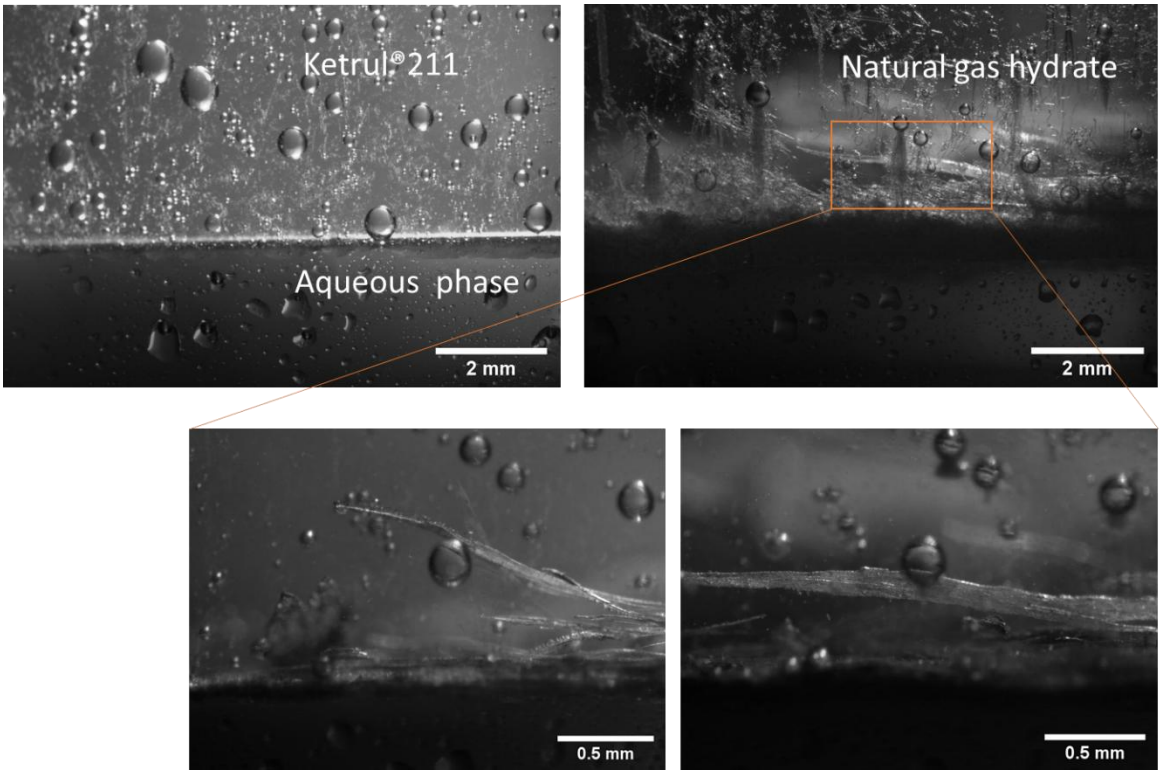

Figure 7 : Needle crystals growth in reactor with a volume of 300 mL, macroscopic scale.

Raman: hydrate micro-imaging

As shown in Figure 8, Raman measurements have been carried out for the reference's phases, that are gas methane phase, methane hydrates solid phase, the aqueous liquid phase with 7 % wt. AA additive and the ketrul211® organic liquid phase. It allows to identify characteristic Raman signatures, necessary for disentangling the various components in such a complex system in the subsequent Raman imaging analysis. For methane hydrates Raman spectrum (Figure 8), the Raman bands ranging from 3000 to 3600 cm^{-1} corresponds to water stretching vibration modes of the methane hydrate crystalline solid phase, and the methane gas molecules encapsulated in the large and small hydrates cages corresponds to the bands 2905 and 2915 cm^{-1}, respectively[26]. The characteristic Raman bands selected for identifying the Ketrul211® condensate phase are observed at 2864 and 2925 cm^{-1} (Figure 8). For the aqueous phase with 7 % wt. AA additive, the Raman bands between 3000 to 3600 cm^{-1} correspond to the water liquid phase and the bands at 2847, 2910 and 2943 cm^{-1} correspond the AA additive.

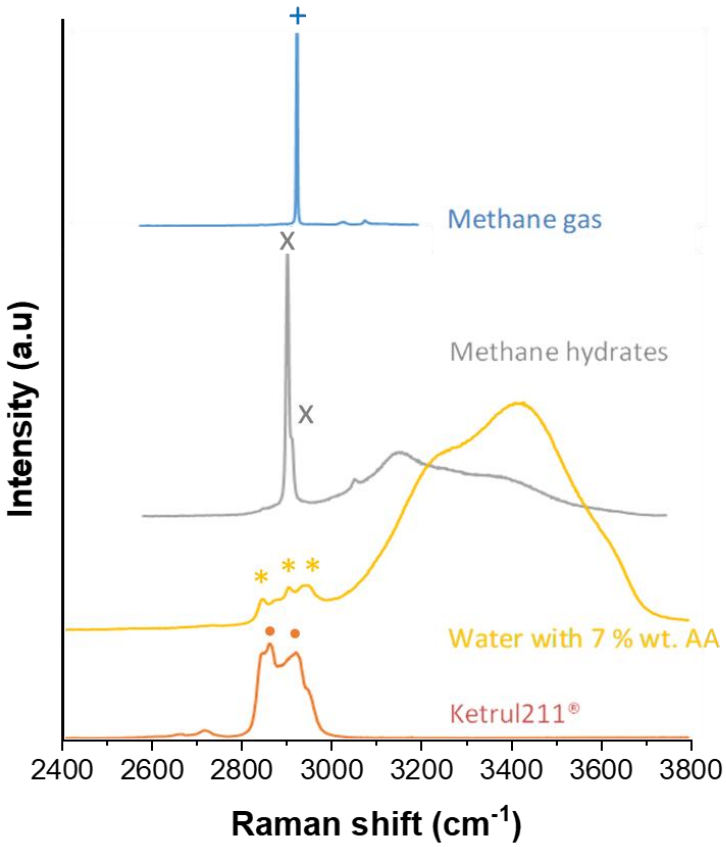

Figure 8 : Raman spectrum for reference phases. The plus sign (+) corresponds to methane gas band measured at 2917 cm^{-1}. The crosses correspond to the characteristic bands of the methane molecules encapsulated in large and small cages at 2905 and 2915 cm^{-1}, respectively. The asterisks correspond to the characteristic Raman bands of AA additive in aqueous phase at 2847, 2910 and 2943 cm^{-1}. The filled circles correspond to the characteristic Raman bands of the Ketrul211® condensate phase at 2864 and 2925 cm^{-1}.

As described in the optical image analyses and in the experimental details, the Raman analysis has been conducted on the methane hydrates formed in thin capillary at 274 K and 70 bar. 2D Raman mapping have been realized on selected hydrates zones where no hydrates movement was observed during the Raman acquisition (lasting *ca.* 7 hours). The 2D mapping couldn't been applied on the surface of polygonal and needle crystals previously described with the help of the optical image analysis, because of their continuous growth on the timescale of the experiment. Typical Raman spectra recorded on these crystals are characteristic of a single phase made of methane hydrate (provided in the supplementary materials). 2D Raman mapping of 40 x 30 µm dimensions (with 1 µm

pixel size) has been acquired on the methane hydrate zone shown as green square in the Figure 5 for the water/ketrul211®/methane system with AA additive. By integrating the characteristic bands of the methane hydrate (water stretching modes between 3000 and 3600 cm^{-1}) and of the ketrul211® (at 2864 and 2925 cm^{-1}) previously discussed, the hydrate/ ketrul211® intensity ratio has been measured for each pixel of the Raman mapping, allowing to construct the Raman image shown in Figure 9a (details about Raman mapping processing are provided in the supplementary materials). Two main zones can be observed: the hydrate-rich zone represented by the light green pixels and the ketrul211®-rich zone represented by the dark green pixels. Figure 9b shows the Raman spectrum of the hydrate-rich zone: it has a high hydrate/ketrul211® intensity ratio. Figure 9c also shows the ketrul211®-rich zone, where the hydrate/ ketrul211® intensity ratio is low. Furthermore, it is worth noting that the profile of the water stretching bands in both zone is characteristic of a crystalline arrangement of the water molecules[27] (for comparison, one may compare the profile for the methane hydrate and 7% wt. aqueous solution samples on Figure 8). Thus, the methane hydrate phase has been characterized inside the continuous ketrul211® liquid phase via 2D Raman mapping thanks to the hydrate to ketrul211® bands ratio. It reveals the formation of methane hydrates aggregates inside the ketrul211® bulk phase matrix.

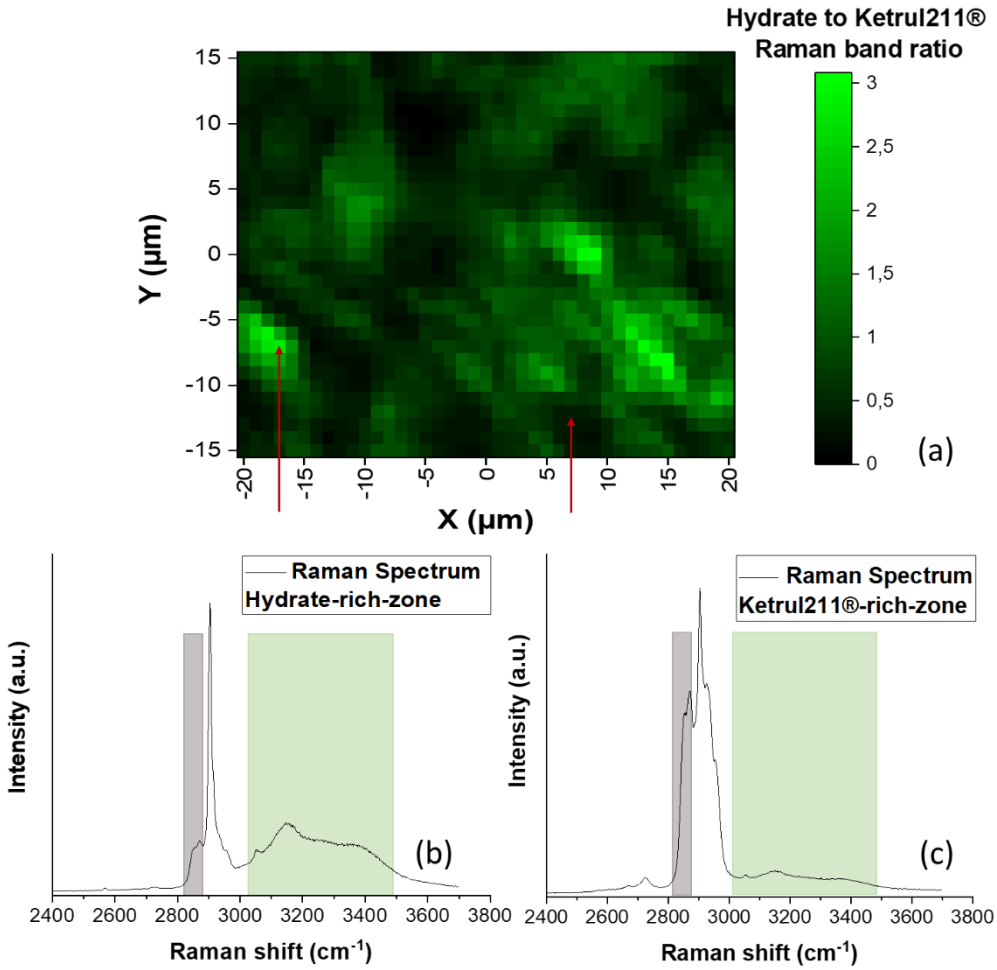

Figure 9 : (a) Raman 2D mapping for methane hydrates formed in the presence of 7 % wt. AA additive. (b) Raman spectrum for hydrate-rich-zone. (c) Raman spectrum for ketrul211®-rich-zone.

IV- Discussion

This study investigates methane hydrate formation at the water/methane and water/ketrul211®/methane interfaces in the presence of the amphiphilic anti-agglomerant additive (AA). The purpose was to study the AA additive mechanism by analyzing its impact on crystal size and

shape at microscopic scale. In addition, the hydrates morphologies were compared to the available natural gas hydrates morphology and size obtained at a macroscopic scale.

Impact of AA additive on the crystal morphology

For the water/methane system without additive, gas hydrates are formed at the water/methane interface, then a hydrate layer develops along the inner wall of the capillary toward methane gas phase. The hydrate layer separates the bulk aqueous phase from methane phase and prevents further crystallization, leading to partial conversion of the water/methane phase into methane hydrate on the timescale of the observation. These observations suggest that an impermeable hydrate layer has been developed at the water/methane interface that blocks mass transfer and stops the crystallization[2].

For the water/methane system with 5 to 7 % wt. AA additive, methane hydrates formation is initiated at the water/methane interface, then the aqueous phase is drawn by capillary forces at the wall towards the methane hydrate growing phase and leads to further crystallization. From the Raman band profile characteristic of the water arrangement (between 3000 to 3600 cm^{-1}), no liquid water phase has been observed in the sample. The presence of AA additive leads to 100 % hydrate conversion rate, thanks to its activity at the water/methane interface maintaining fluid mass transfer during methane hydrate formation. This is achieved as AA additive adsorb at the water/methane interface, as observed through the reduction of the surface tension from 65.79 (without AA) to 29.20 mN/m (with AA). This indicates the saturation of water/methane interface by adsorbed AA additive molecules and the saturation of water phase by AA additive dispersed micelles (CMC 0.004 % wt).

The presence of AA additive leads to polygonal periodic crystals in water/methane system. The size of small crystals is close to 2 µm, whereas the size of big crystals is distributed from 5 to 20 µm. The spectroscopic measurement has been applied through the polygonal crystal of 20 µm from one side to another side. All the Raman band detected between 3000 and 3600 cm^{-1} correspond to crystalline phase. No liquid water bands have been detected. The microscopic observation through the same crystal confirms the presence of homogenous solid phase without liquid water inside the crystal itself. All the polygonal crystals are dense.

For water/ ketrul211®/methane without additive, gas hydrates start formed at the water/ketrul211® interfaces, and then a hydrate layer develops along the capillary walls and covered the walls on the entire ketrul211® phase height. This hydrate layer growth continuously from the water/ketrul211® interface up to the ketrul211®/methane interface, and then crystallization stops. The capillary is hydrophilic. The water phase has been drawn up to the capillary walls by capillary forces, covered the ketrul211® phase and converted to methane hydrate at 70 bar and 274 K.

The presence of AA additive leads to hydrate formation at the water/ketrul211® interface and the growth of needle-like crystals in the ketrul211® phase towards the methane phase. The ketrul211® contains the dissolved methane that afford the methane molecules needed to stabilize hydrates. The needle size is close to a length of 10 µm. The needles develop continuously from the water/Ketrul211® interface to the ketrul211®/methane interface. Without AA additive the hydrate layer develops on the capillary walls and covered the ketrul211® phase. The AA additive activity at the water/ ketrul211® interface ensure the methane and water mass transfer to the hydrate surface for continuous crystallization in the ketrul211® phase. The AA additive adsorbs at the water/ketrul211® interface and reduces the interfacial tension from 42.00 to 0.81 mN/m. The saturation of water/ketrul211® interface by AA additive adsorbed molecules and the formation of AA additive dispersed micelles in the water phase act as molecules reservoir to act as methane solubilizer and shape modifier by absorption on the growing crystal.

The impact of AA additive on crystal morphology is observed macroscopically in 300 mL reactors. Crystals has been developed as polygons in the water and needles in the ketrul211® phase. Here, the crystal's size is close to a few millimeters. At macroscopic and microscopic scales, similar methane hydrates crystals morphology has been observed: polygonal crystals in water and needle crystals in ketrul211®. The methane hydrate crystals are fractal objects formed in the presence of AA additive,

where the polygonal and needle grow in periodic unit from microscopic to macroscopic scale inside the reactors.

According to the literature[23], the solute saturation inside the solvent can impact the crystal shape. The crystals growth as a polygonal shape where α-amylase concentration is low in aqueous phase. The crystal change morphology as a needle shape where the α-amylase protein concentration became high in the water. Here, from low to high solute saturation the crystal morphology changes from polygonal to needle[23]. In this case, the protein α-amylase represents the solute. However, for methane hydrate crystals, both water and methane molecules represent the solute. By this, the water high concentration and methane low concentration in the aqueous phase is probably the reason for polygon methane crystal shape in water. In the same way, the methane high concentration and water low concentration in the ketrul211® phase can lead probably to needle crystals in this organic liquid phase. However, this hypothesis is only valid in the presence of AA additive, since in the absence of the anti-agglomerant additive, there is no polygonal or needle crystals developed in macroscopic or microscopic scale. Evidently, the crystals morphology is related to two parameters, at least: first, the methane and water saturation in the ketrul211® and aqueous phases, and secondly the adsorption mechanism of the anti-agglomerant (Amphiphilic AA additive) at the water/ketrul211® and at the ketrul211®/hydrate crystals interfaces.

Several studies show that the additives adsorption on the hydrate crystals can control their morphologies. Below the critical micellar concentration, the surfactant Tween 65 leads to planar shell cyclopentane crystals. Above this critical concentration, the surfactant Tween 65 control cyclopentane hydrates morphology from planar shell to conical shape[28]. The Tween 65 adsorption mechanism at water/cyclopentane interface and its concentration control the hydrate cyclopentane morphology. In the same way, another study[10,11] from the literature explains that the presence of the additive Noramium DA 50 surfactants at 0.1 % wt. concentration and salinity of 4% wt. NaCl, leads to pyramidal cyclopentane hydrates crystals at the water/cyclopentane interface where the cyclopentane crystals are pointed towards the cyclopentane phase. Conversely, the absence of Noramium DA 50 surfactant lead to cyclopentane hydrate formation at the water/cyclopentane interface as layer covering the entire surface between the two phases[10,11]. The Noramium DA 50 surfactant makes the cyclopentane crystals wettable to the organic phase. The authors[10,11] suggested that the adsorption mechanism of surfactants controls the cyclopentane crystal morphology, whereas the surfactant Tween 65 leads to planar-shell shape and Noramium DA 50 leads to pyramidal shape. Here, both surfactants have different chemical structure (Noramium DA50© is a quaternary ammonium surfactant and Tween 65 is a sorbitan ester nonionic surfactant). Consequently, the adsorption mechanism is linked to their chemical structure and induces different crystal shape.

For approaching the gas hydrates formation in pipelines, few studies have been carried out with methane/propane hydrates formation in a water/n-octane system. The absence of surfactant leads to hydrate layer formation at the water/n-octane interface. With 0.1 % Noramium DA 50 and 4 % wt. NaCl, crystals develop at the water/n-octane interface as a pyramidal shape oriented towards the n-octane (the organic phase). Consequently, the methane/propane hydrates became oil-wettable in the presence of the surfactant Noramium DA 50. To validate that the Noramium DA 50 activity is the only parameter that control the hydrates morphology, complementary measurements have been carried out using different organic phases: cyclopentane, n-octane, mixed cyclopentane/n-octane, and mixed cyclopentane/n-dodecane. For all the systems, pyramidal crystals have grown in organic phases[10,11]. The surfactant Noramium DA 50 adsorption mechanism at the hydrate surface control the crystal growth for methane/propane hydrates and cyclopentane hydrates no matter whether the guest molecule is a gas molecule or a liquid one (cyclopentane)[10,11]. Results obtained lead to propose the hydrate growth mechanism in the presence of Noramium DA 50 of 0.1 to 1 wt % and 4 % wt. NaCl: first, formation of hydrates crystals at the water/cyclopentane interface saturated with Noramium DA 50. Second, adsorption of Noramium DA 50 on the crystals. Third, vertical growth by conversion of the pre-melting layer that surround the crystal to hydrates. Then, third step repeated right up to vertex. Finally, full coverage of water/CP by pyramidal crystal[11].

The adsorption mechanism of additives on hydrates crystals depends on their chemical structure. By this, the surfactant (Tween 65 or Noramium DA 50) and anti-agglomerant (Amphiphilic AA additive) have different chemical structures. They both have different adsorption mechanism and consequently hydrate inhibition, even if they all decrease superficial and interfacial tensions between water and organic phase. However, in the present study, the anti-agglomerant additive does not stabilize emulsions like surfactants. Under stirring, the presence of anti-agglomerant additive allows aqueous phase to be dispersed as a droplet in the organic phase. Without stirring, the organic and aqueous phases separate in less than 10 s. The hydrophilic/hydrophobic characters lead to adsorption on the crystals with both types of chemicals, but the resulting crystal size and shapes obtained are different and probably linked to the chemical structures the type of additives.

The diffusion rate of gas impacts the hydrate growth rate and to a certain extend also control crystal morphology. According to the literature, from low to high methane diffusion rates, gas hydrate crystal morphology changes from polygonal to dendritic shape[24-25]. Increasing subcooling results in increasing driving force and speed up methane mass transfer towards hydrate surface, consequently it increases the crystal growth rate which controls the crystal shape and morphology. At a low subcooling temperature of 3 K, the hydrate growth rate is 0.1 mm/min. At 6 K subcooling the hydrate growth rate increases to 10 mm/min[24-25]. Furthermore, at high subcooling, the crystal surface decreases compared to the crystal surface at low subcooling temperature[29]. The gas diffusion rate represents a second parameter that control the crystal size and morphology.

To sum up, the gas diffusion rate and the additives adsorptions mechanism both control the size and morphology of hydrate crystals. In this study, polygonal crystal shapes in water phase and needle hydrate crystal shapes in ketrul211® phase were observed. They are the results of a competition mechanism between the methane availability/diffusion rate and the AA additive adsorption mechanism at water/methane and water/ketrul®211 interfaces. In the water phase, from 1 to 7 % wt. AA additive concentration and low methane content, the crystal growth is slow from hours to days, consequently, hydrate growth with a wide surface as polygonal shape. While, in ketrul211® organic phase, 1 to 7 % of AA additive and high methane content lead to a rapid growth rate of crystal within few minutes. Consequently, hydrates grow with a thin surface such as needle shape.

Impact of AA additive on the hydrate rich zone

The impact of AA additive has been studied for water/methane and water/ketrul211®/methane systems. Measurements have been carried out via Raman spectroscopy and imaging. For water/methane system, the methane hydrate and methane gas distribution in the hydrate-rich-zone have been evaluated around 50 % (Table 2). In the presence of the AA additive, the methane hydrate and methane gas distribution has been determined at 47-49 % (Table 2). Here, the hydrate and methane gas distribution represent hydrate to methane Raman band ratio inside the 2D mapping of 40 x 30 µm dimension and pixel size of 1 µm (Supplementary materials). The presence of AA additive has no significant effect for the hydrate-rich-zone formed for water/methane system. This is because the 2D mapping can only be applied on homogeneous concentrated and immobile hydrate zones for Raman measurements.

Similar analysis has been applied on methane hydrate matrix for the water/methane system, in the presence of sodium dodecyl sulfate (SDS®) surfactant[20]. In this case, the hydrates grew by SDS® water solution imbibition of an already formed crystals. This water layer is instantaneously (seconds or less) transformed into hydrate and the process continued until no more water was available for crystallization. The resulting “massive” hydrates block formed presents a porous structure and the two - dimensional mapping have been applied for 70 x 50 µm dimensions and 3 µm pixel size. For a concentration of 500 ppm, the hydrate matrix porosity has been estimated close to 60 – 80 % and pores size close to 30 µm. The pores were filled with aqueous solution[20].

When compared with water/methane systems with AA additive which form dispersed accumulated hydrates. It is difficult to talk about porosity because the AA aims at forming tiny, more or less, isolated hydrates particles. The 50 % concentration of the methane-hydrate-rich-zone formed is lower than the

60 - 80% porosity of the methane-hydrate-matrix formed in the presence of SDS® surfactant. For the accumulated hydrate-rich-zone obtained in presence of AA additive the surface zone between particles is around 5 x 5 µm. For the hydrate-rich-zone obtained in the presence of the SDS® surfactant, the pore size is 10 x 30 µm. These two additives, AA additive and SDS®, are fundamentally different in the way they interact with methane hydrates. Progressive layer of hydrates on an existing particles or block of hydrates formed with a very rapid growth rate (seconds or less) on one side and formation of dispersed small movable particles on the other side.

This leads to the conclusion that not all the surfactant acts the same way on the morphology of hydrates crystals as discussed for Noramium DA 50®/Tween 65®/SDS®. Each additive leads to a different hydrate system. Smalls and massive hydrate particles are obtained in the presence of the AA additive, massives and porous hydrates zones are obtained in the presence of the SDS® surfactant.

By using the Raman measurement, the gas hydrates-rich-zone accumulation in presence of ketrul211® organic liquid phase has also been investigated (Figure 9a). When AA additive is added movable needles grew in the condensate and accumulation of hydrates particles are formed above the water/ketrul211® interface (see Figure 5). As explained previously, the 2D mapping analysis had been possible only on the hydrates accumulation near the water/ketrul211® interface where hydrates remain immobile during the 7 hours Raman acquisition. The hydrate-rich-zone presents similar hydrate-rich-zone ratio (50 %) than the system without AA (Table 2). We suggest that this ratio would have been notably different if it was possible to evaluate it on the single needle crystal on a smaller dimension of 5x5 µm.

V- Conclusion

In this study, the impact of amphiphilic anti-agglomerant commercial additive has been investigated on the methane hydrate morphology and aggregate size by using Raman spectroscopy and optical imaging. The hydrate formation has been carried out within a thin capillary of 200 µm diameter by considering water/methane and water/ketrul211®/methane systems at 70 bar and 274.15 K and using aqueous phase with a salinity of 5 g/L NaCl and AA additives at various concentrations (5 and 7 % wt.). In parallel, gas hydrate formation was carried out at macroscopic scale by using high pressure reactor of 300 mL and the resulting hydrate growth and morphology were analyzed by optical images. Optical macroscopic and microscopic Raman data analysis reveals that the AA additive has an impact on the morphology of methane hydrate crystals, leading to polygon periodic crystal formation in the water phase (crystal size in order of 1 to 10 µm) and needle crystal perpendicular formation in the ketrul211® organic phase (crystal size close to 10 µm). By means of Raman spectroscopy, in the presence of AA additive, the hydrate distribution in ketrul211® (which refers to the Raman bands ratio of hydrates to ketrul211®) is estimated at 50% for both water/methane and water/ketrul211®/methane systems. This study suggests that the gradient of methane diffusion rates could provide insights into the methane hydrate growth rate. In general, good AA must change the wettability and ensure the dispersibility of the particles. Consequently, two main parameters should be considered as they impact the crystal shape and size: the gas availability and the additive effect. The morphology change seems to be a consequence of the AA effect and not the main targeted mechanism to dispersed hydrate (see for example a study on AA structure and dispersibility[3]). Besides, a constant characteristic of all AA we have tested is the very high water to hydrate conversion rate. It means that the free water is almost negligible in the system. In addition, possibly AA ammonium active materials will enhance the formation of numbers of very small and isolated particles that will avoid the growth of big objects. This investigation has been conducted on methane-based systems and additional investigations may be performed by using natural gas hydrates for better reproducing the conditions met in oil and gas offshore production.

Acknowledgement

The authors are grateful to TotalEnergies OneTec, IFP Energies Nouvelles and Groupe Spectroscopie Moléculaire ISM UMR 5255 for their financial and scientific support.

Supporting Information Available

Micro differential scanning calorimeter; Raman Spectroscopy and estimation of phases distribution

References

(1) Sloan, E.D., Koh, C.A. *Clathrate Hydrates of Natural Gases,* 3rd ed.; Chemical Industries; CRC Press, **2007**. DOI: 10.1201/9781420008494

(2) Broseta, D., Ruffine, L., Desmedt, A. *Gas Hydrates 1: Fundamentals, Characterization and Modeling*. ISTE Ltd, **2017**. DOI: 10.1002/9781119332688

(3) Hu, S., Vo, L., Monteiro, D., Bodnar, S., Prince, P., Koh, C.A. Structural Effects of Gas Hydrate Antiagglomerant Molecules on Interfacial Interparticle Force Interactions, *Langmuir*, **2021**, *37* (5), 1651–1661. DOI: 10.1021/acs.langmuir.0c02503

(4) Zhao, H., Sun, M., Firoozabadi, A. Anti-agglomeration of natural gas hydrates in liquid condensate and crude oil at constant pressure conditions, *Fuel*, **2016**, *180*, 187–193. DOI: 10.1016/j.fuel.2016.03.029

(5) Aman, Z.M., Koh, C.A. Interfacial phenomena in gas hydrate systems, *Chemical Society reviews*, **2016**, *45*, 1678–1690. DOI: 10.1039/C5CS00791G

(6) Glenat, P., Pagezy, L., Devoisselle, R., Bourg, P., Pere, M., Melchuna, A. Rheological study of liquid hydrates slurries in presence of commercial hydrates dispersants (AA-LDHIs) *Paper presented at the 9th International Conference on Gas Hydrates (ICGH)*, Denver, Colorado, USA, June **2017**.

(7) Kelland, M.A. History of the Development of Low Dosage Hydrate Inhibitors, *Energy & Fuels*, **2006**, *20* (3), 825–847. DOI: 10.1021/ef050427x

(8) Patel, Z.D., Dibello, M., Fontenot, K., Guillory, A., and Hesketh-Prichard, R. Continuous Application of Anti-Agglomerant LDHI for Gas-Condensate Subsea Tieback Wells in Deepwater Gulf of Mexico, *Paper presented at the Offshore Technology Conference*, Houston, Texas, USA, May **2011**. DOI: 10.4043/21836-MS

(9) Frostman, L. M., Przybylinski, J. L. Successful Applications of Anti-agglomerant Hydrate Inhibitors, *Paper presented at the SPE International Symposium on Oilfield Chemistry*, Houston, Texas, USA, February **2001**. DOI: 10.2118/65007-MS

(10) Delroisse, H., Torré, J.P., Dicharry, C. Effects of a Quaternary Ammonium Salt on the Growth, Wettability, and Agglomeration of Structure II Hydrate Crystals, *Energy & Fuels,* **2018**, *32* (12), 12277–12288. DOI: 10.1021/acs.energyfuels.8b02980

(11) Delroisse, H., Torré J.P., Dicharry, C. Effect of a Hydrophilic Cationic Surfactant on Cyclopentane Hydrate Crystal Growth at the Water/Cyclopentane Interface, *Crystal Growth & Design*, **2017**, *17* (10), 5098–5107. DOI:10.1021/ACS.CGD.7B00241

(12) Beltran, J. G., Servio, P. Morphological Investigations of Methane−Hydrate Films Formed on a Glass Surface, *Crystal Growth & Design*, **2010**, *10* (10), 4339–4347. DOI: 10.1021/cg1003098

(13) Martinez de Banos, M. L., Hobeika, N., Bouriat, P., Broseta, D., Enciso, E., Clement, F., Brown, R. How Do Gas Hydrates Spread on a Substrate, *Crystal Growth & Design*, **2016**, *16* (8), 4360–4373. DOI: 10.1021/acs.cgd.6b00471

(14) Hassanpouryouzband, A., Joonaki, E., Vasheghani Farahani, M., Takeya, S., Ruppel, C., Yang, J., English, N.J., Schicks, J.M., Edlmann, K., Mehrabian, H., Aman, Z.M., Tohidi, B. Gas hydrates in sustainable chemistry, *Chemical Society reviews*, **2020**, *49*, 5225–5309. DOI: 10.1039/C8CS00989A

(15) Zhong, Y., Rogers, R. E. Surfactant effects on gas hydrate formation, *Chemical Engineering Science*, **2000**, *55* (19), 4175–4187. DOI: 10.1016/S0009-2509(00)00072-5

(16) Gayet, P., Dicharry, C., Marion, G., Graciaa, A., Lachaise, J., Nesterov, A. Experimental determination of methane hydrate dissociation curve up to 55MPa by using a small amount of surfactant as hydrate promoter, *Chemical Engineering Science*, **2005**, *60* (21), 5751–5758. DOI: 10.1016/j.ces.2005.04.069

(17) Watanabe, K., Imai, S., Mori, Y.H. Surfactant effects on hydrate formation in an unstirred gas/liquid system: An experimental study using HFC-32 and sodium dodecyl sulfate, *Chemical Engineering Science*, **2005**, *60* (17), 4846–4857. DOI: 10.1016/j.ces.2005.03.043

(18) Okutani, K., Kuwabara, Y., Mori, Y.H. Surfactant effects on hydrate formation in an unstirred gas/liquid system: An experimental study using methane and sodium alkyl sulfates, *Chemical Engineering Science*, **2008**, *63* (1), 183–194. DOI: 10.1016/j.ces.2007.09.012

(19) Molokitina, N.S., Nesterov, A.N., Podenko, L.S., Reshetnikov, A.M. Carbon dioxide hydrate formation with SDS: Further insights into mechanism of gas hydrate growth in the presence of surfactant, *Fuel*, **2019**, *235*, 1400–1411. DOI: 10.1016/j.fuel.2018.08.126

(20) Venet, S., Guerton, F., Desmedt, A., Broseta, D. Insights into the porous structure of surfactant-promoted gas hydrate, *Chemical Engineering Science*, **2022**, *248*, 117193. DOI: 10.1016/j.ces.2021.117193

(21) Sinquin, A., Cassar, C., Teixeira, A., Leininger, J.P., Glénat, P. Hydrate Formation in gas Dominant systems, *Offshore Technology Conference and Exhibition*, Ravenna, Italy; Paper OMC-2015-416.

(22) Sinquin, A., Gainville, M., Cassar, C., Boxall, J., Estanga, D. Evaluation of Anti-Agglomerant hydrate inhibitors in gas-dominated system under different flow regimes, *11th North American Conference on Multiphase Production Technology*, Banff, Canada, BHR-2018-125.

(23) Boistelle, R., Astier, J.P. Crystallization mechanisms in solution, *Journal of Crystal Growth*, **1988**, *90* (1-3), 14–30. DOI: 10.1016/0022-0248(88)90294-1

(24) Ohmura, R., Matsuda, S., Uchida, T., Ebinuma, T., Narita, H. Clathrate Hydrate Crystal Growth in Liquid Water Saturated with a Guest Substance: Observations in a Methane + Water System, *Crystal Growth & Design*, **2005**, *5* (3), 953–957. DOI: 10.1021/cg049675u

(25) Ohmura, R., Shimada, W., Uchida, T., Mori, Y.H., Takeya, S., Nagao, J., Minagawa, H., Ebinuma, T., Narita, H. Clathrate hydrate crystal growth in liquid water saturated with a hydrate-forming substance: variations in crystal morphology, *Philosophical Magazine*, **2004**, *84* (1), 1–16. DOI: 10.1080/14786430310001623542

(26) Sum, A. K., Burruss, R. C.; Sloan, E. D. Measurement of clathrate hydrates via Raman spectroscopy, *The Journal of Physical Chemistry B*, **1997**, *101*, 7371–7377. DOI: 10.1021/JP970768E

(27) Chazallon, B, Noble, J.A., Desmedt, A. Spectroscopy of Gas Hydrates: From Fundamental Aspects to Chemical Engineering, *Geophysical and Astrophysical Applications*, WILEY, **2017**, 63–112. DOI: 10.1002/9781119332688.ch2

(28) Dann, K., Rosenfeld, L. Surfactant Effect on Hydrate Crystallization at the Oil-Water Interface, *Langmuir*, **2018**, *34* (21), 6085–6094. DOI: 10.1021/acs.langmuir.8b00333

(29) Saito, K., Kishimoto, M., Tanaka, R., Ohmura, R. Crystal Growth of Clathrate Hydrate at the Interface between Hydrocarbon Gas Mixture and Liquid Water, *Crystal Growth & Design*, **2011**, *11* (1), 295–301. DOI: 10.1021/cg101310z

TOC Graphic

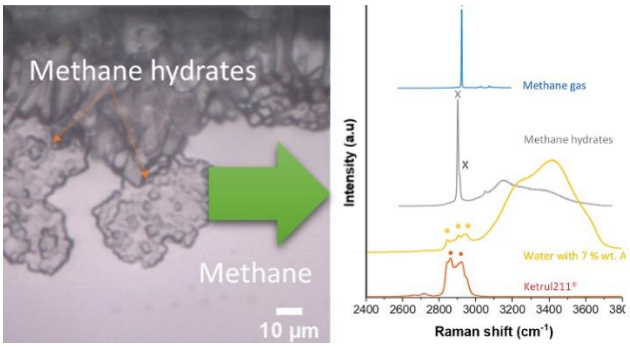
Methane hydrates
Methane
10 µm
Methane gas
Methane hydrates
Water with 7 % wt. A
Ketrul211®
Intensity (a.u)
2400 2600 2800 3000 3200 3400 3600 380
Raman shift (cm-1)